







Global biomass fires and infant mortality

Hemant K. Pullabhotla^{a,b,1} , Mustafa Zahid^a , Sam Heft-Neal^a , Vaibhav Rathi^c, and Marshall Burke^{a,d,e} 

Edited by B. Turner, Arizona State University, Tempe, AZ; received October 25, 2022; accepted May 1, 2023

Global outdoor biomass burning is a major contributor to air pollution, especially in low- and middle-income countries. Recent years have witnessed substantial changes in the extent of biomass burning, including large declines in Africa. However, direct evidence of the contribution of biomass burning to global health outcomes remains limited. Here, we use georeferenced data on more than 2 million births matched to satellite-derived burned area exposure to estimate the burden of biomass fires on infant mortality. We find that each additional square kilometer of burning is associated with nearly 2% higher infant mortality in nearby downwind locations. The share of infant deaths attributable to biomass fires has increased over time due to the rapid decline in other important causes of infant death. Applying our model estimates across harmonized district-level data covering 98% of global infant deaths, we find that exposure to outdoor biomass burning was associated with nearly 130,000 additional infant deaths per year globally over our 2004 to 2018 study period. Despite the observed decline in biomass burning in Africa, nearly 75% of global infant deaths due to burning still occur in Africa. While fully eliminating biomass burning is unlikely, we estimate that even achievable reductions—equivalent to the lowest observed annual burning in each location during our study period—could have avoided more than 70,000 infant deaths per year globally since 2004.

air pollution | infant mortality | biomass fires

Globally, an estimated four million square kilometers of vegetation burns each year (1, 2). These outdoor biomass fires emit various aerosols, greenhouse gases, and a variety of hazardous trace gases with significant air quality implications. Biomass fires are estimated to contribute nearly 62% of global particulate organic carbon, 27% of black carbon (3), 32% of carbon monoxide, and 40% of carbon dioxide (4), and form the single largest source of fine particulate matter (PM_{2.5}) in many developing countries (5, 6). However, the relative contributions of biomass burning to regional air quality depend on the magnitude of emissions from other sources and vary with trends in burning, which show broad regional heterogeneity over the last two decades. For example, Africa has seen an estimated 18.5% decline in the total burned area, 80% of which occurred in Northern Hemisphere Africa. Conversely, fire activity is estimated to have increased in many areas of South and Southeastern Asia, likely due to increased adoption of agricultural residue burning practices (7, 8).

Levels and trends in biomass burning are substantially attributable to human activity (1, 9), either directly, as in tropical regions where land clearing or residue burning is common, or indirectly, as in temperate or boreal forests where anthropogenic climate change is rapidly amplifying wildfire risk (10). Given the human role in these fires, their large associated pollutant emissions, the often distant transport of these pollutants into populated areas, and growing evidence from local or regional studies on the health impacts of such burning (11–14), understanding the implications of global biomass burning is critical for designing optimal environmental regulations and public health policies.

Yet accurately quantifying exposures to smoke from biomass burning and the impacts of these exposures on health remain challenging, particularly at large spatial scales. First, biomass burning results in a wide variety of emissions, complicating atmospheric model-based approaches to measuring the health impacts of burning. Biomass fires result in gases such as carbon dioxide, carbon monoxide, ozone, and nitrogen oxides, as well as pollutants such as particulate matter and persistent organic pollutants such as polycyclic aromatic hydrocarbons (PAHs) and polychlorinated dibenzo-p-dioxins and dibenzofurans (PCDD/Fs) (15–17). Each of these pollutants is likely to have separate and additive human health impacts through multiple biological channels. Emissions from biomass burning are also poorly constrained empirically, resulting in high levels of uncertainty in modeling approaches that use emissions inventories to study impacts (18, 19). Additionally, to estimate health impacts, modeled emissions are often combined

Significance

Outdoor burning of forest, grassland, and agricultural biomass is a significant contributor to air pollution globally. Here, we empirically estimate the impact of exposure to such biomass burning on infant mortality. We find that an additional square kilometer of burning is associated with nearly 2% higher infant mortality in nearby downwind locations. Applying our estimates to a global sample of 105 countries, we find that even conservative reductions in burning could contribute to more than 70,000 avoided infant deaths annually.

Author affiliations: ^aCenter on Food Security and the Environment, Stanford University, Stanford, CA 94305; ^bDepartment of Economics, Deakin University, Burwood, VIC 3125, Australia; ^cDepartment of Economics, Stockholm University, Stockholm 106 91, Sweden; ^dDoerr School of Sustainability, Stanford University, Stanford, CA 94305; and ^eNational Bureau of Economic Research, Cambridge, MA 02138

Author contributions: H.K.P. and M.B. designed research; H.K.P., M.Z., S.H.-N., V.R., and M.B. performed research; H.K.P., M.Z., S.H.-N., and V.R. analyzed data; and H.K.P., M.Z., S.H.-N., and M.B. wrote the paper.

The authors declare no competing interest.

This article is a PNAS Direct Submission.

Copyright © 2023 the Author(s). Published by PNAS. This article is distributed under [Creative Commons Attribution-NonCommercial-NoDerivatives License 4.0 \(CC BY-NC-ND\)](https://creativecommons.org/licenses/by-nc-nd/4.0/).

Although PNAS asks authors to adhere to United Nations naming conventions for maps (<https://www.un.org/geospatial/mapsgeo/>), our policy is to publish maps as provided by the authors.

¹To whom correspondence may be addressed. Email: h.pullabhotla@deakin.edu.au.

This article contains supporting information online at <http://www.pnas.org/lookup/suppl/doi:10.1073/pnas.2218210120/-DCSupplemental>.

Published May 30, 2023.

with health dose–response relationships that are mainly derived from data in wealthy regions, and these functions might not accurately characterize responses in low- and middle-income countries where comorbidities differ, and both mortality rates and average ambient PM_{2.5} concentrations are typically much higher. Consequently, estimates of the health impacts of biomass burning that rely on modeled emissions likely provide an incomplete assessment of the actual health costs of exposure to burning.

A second challenge is to separate the pollution-driven health impacts of fires from other socioeconomic factors correlated with fire activity. As noted, vegetation fires are predominantly anthropogenic, with more than 90% of overall fire activity estimated to have human-induced causes (1, 9). Thus, accurately quantifying the health impacts of biomass fires requires disentangling the likely negative effects of the pollution they generate from the potential health or livelihood benefits of the economic activity with which they are associated. A few recent studies circumvent these challenges in estimating the impact of fires on health outcomes (11–14). However, these studies are limited to narrow geographies. Existing studies at a region or global scale primarily rely on exposures from chemical transport model simulations and empirical frameworks that are not well equipped to isolate health impacts from other covarying factors (6, 20, 21). Consequently, the global health implications of outdoor biomass burning and its changing patterns in recent years remain unclear.

Here, we quantify the impact of exposure to biomass burning on infant health by combining satellite measures of burned area with geolocated household survey data on infant mortality from nationally representative Demographic and Health Surveys (DHS). Our approach of characterizing exposure as the observed burned area in the vicinity offers several empirical advantages over using modeled biomass fire emissions. First, it limits the measurement error that could arise from using chemical transport or dispersion models that often rely on uncertain underlying parameterization or emissions inventories (19). Second, our

estimated effect reflects the overall impact of exposure to biomass fires, accounting for all varieties of pollutants present in the smoke from vegetative matter combustion. This provides a more accurate assessment of the net health damages from biomass fires rather than the effect of any one single pollutant associated with emissions from fires. An additional advantage of the burned area measure is that it provides a transparent and direct link to an outcome over which policymakers, in principle, could have direct influence.

We use infant mortality data from 116 Demographic and Health Surveys (DHS) representing 54 countries across the developing world and encompassing 2,237,307 births between 2004 and 2018 (Fig. 1 shows the DHS sample countries in white borders. *SI Appendix, Fig. S1* shows the location of births. *SI Appendix, Table S1* lists the DHS surveys in the sample). Using survey information on the location and timing of each birth, we estimate exposure to burned biomass during the nine months leading up to and 12 mo following the month of birth (*Methods*), the period that existing studies suggest is critical for early life outcomes (22). These data constitute our main sample for estimating the impact of the burned area on infant health.

To extrapolate derived estimates beyond countries where DHS data are available, we also compile subnational infant mortality data across 105 countries that fall within the ranges of infant mortality and biomass burned area observed in the estimation sample (*Methods, Fig. 1*). This extended sample encompasses nearly 98% of the total infant deaths and 80% of total biomass burning observed globally between 2003 and 2018. Using estimates derived from the DHS sample, we calculate the infant mortality attributable to biomass burning exposure across these 105 countries, which comprise the bulk of the global population exposed to biomass burning and where an overwhelming majority of infant deaths occur.

Exposure to outdoor vegetation burning can increase infant mortality by increasing exposure to poor air quality. On the

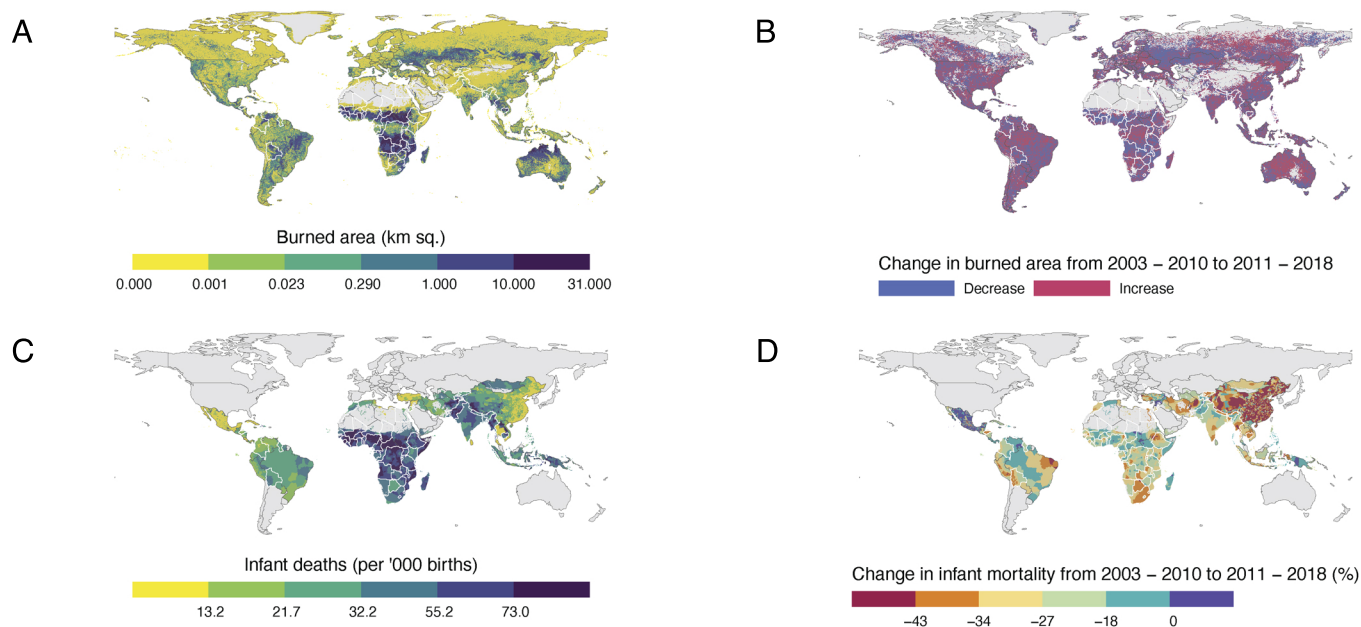


Fig. 1. Global prevalence and change in outdoor vegetation burning and infant mortality (2003 to 2018). (A) Annual average biomass burned area globally 2003 to 2018 (B) Increase or decrease in the average burned area between 2003 to 2010 and 2011 to 2018 (C) Annual average infant mortality rate (deaths per thousand births) 2003 to 2018. (D) Percentage change in infant mortality from 2003 to 2010 to 2011 to 2018. Countries in white borders indicate those with DHS data used in the main estimation. Infant mortality data in C and D are shown for the countries in the extended sample (*Methods*) used for calculating global infant mortality attributable to outdoor biomass burning exposure.

other hand, households may derive income and economic benefits from the activities associated with burning, including preparation or clearing of land for crop or animal agriculture, the procurement of forest services, or other livelihood activities. To isolate the air quality component, we leverage changes in wind direction and compare health impacts when additional area is burned upwind or downwind of a given location (*SI Appendix, Fig. S2*). While both upwind and downwind burned areas could influence economic activity, pollution from upwind burned areas is more likely to be transported to the birth location and reduce air quality. We provide supporting evidence for the relatively large pollution impact from upwind burned areas (compared to downwind burning) by using data on particulate matter pollution from available ground monitors situated in low- and middle-income countries, matched to upwind and downwind burned areas around those monitors.

We estimate the effect of exposure to biomass burning on infant mortality using plausibly exogenous variation in upwind burned area determined by wind direction changes. Specifically, we compare mortality outcomes for different infants who are born in the same location but, given changes in wind direction and burning activity over time, are exposed to different amounts of upwind burning in the months prior to and post birth. We flexibly account for other seasonal or regionally trending factors that could be correlated with both variation in burned area and infant mortality. Our regression models also include controls

for other time-varying local weather conditions (temperature, precipitation, and wind speed) and child, maternal, and household characteristics that affect health outcomes (*Methods*).

Results

We find that postbirth exposure to biomass burning upwind of birth location is associated with an increased risk of infant mortality (Fig. 2*A*). A one square kilometer increase in upwind burned area exposure is associated with a 2.1% increase in infant mortality—an increase of 1.06 (95% CI 0.017 to 2.10) additional deaths per '000 births relative to the sample mean infant mortality rate of 52.5 deaths per '000 births (Fig. 2*A*, *SI Appendix, Table S2*). Effects are driven by fires that are more proximate to birth locations (*SI Appendix, Fig. S3*). In contrast to postbirth exposure, we see no effect of in utero prebirth exposure to biomass burning on infant mortality (*SI Appendix, Fig. S3 and Table S2*). We see positive, albeit noisy, effects of prebirth exposure (overall, or trimester-wise exposure) on neonatal mortality risk within the first month of birth (*SI Appendix, Fig. S4*).

Outdoor vegetation burning that occurs downwind of a birth location has no impact on the risk of infant mortality (Fig. 2*A*). The lack of an effect from downwind burning is consistent with an underlying mechanism of biomass burning impacting infant health through deteriorating air quality. A statistical test of the difference between the upwind and downwind exposure

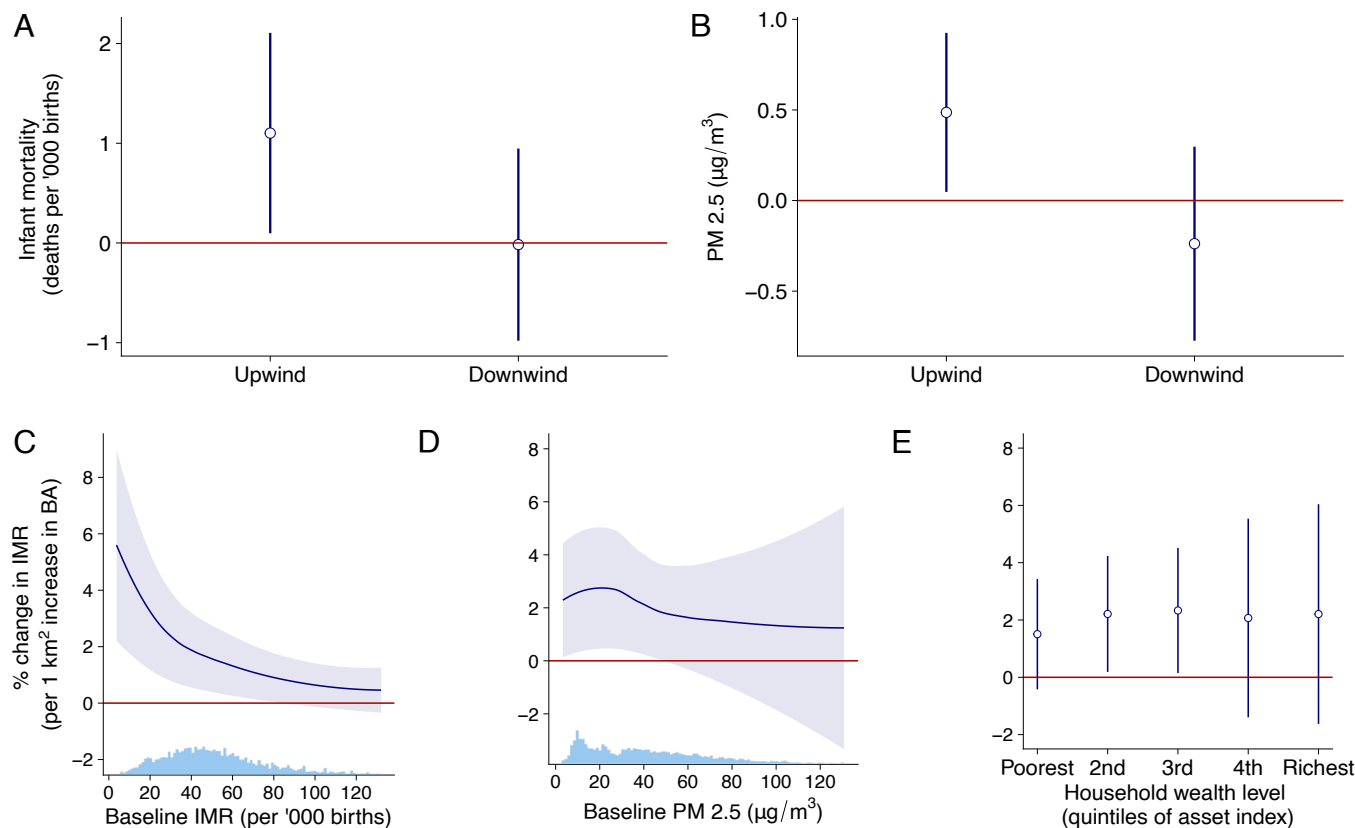


Fig. 2. Burned area, infant mortality, and particulate matter pollution. Exposure to upwind biomass burning is associated with higher *A* infant mortality (IMR) and *B* particulate matter pollution (PM_{2.5}), but downwind burned area is not. Plots in the bottom row show heterogeneity in the impact of biomass burning exposure on infant mortality risk across *C* baseline infant mortality, *D* baseline ambient pollution, and *E* household wealth. *A* and *B* show the marginal effect (coefficients and 95% CI whiskers) of a 1-km square increase in burned area in upwind and downwind directions. Infant mortality estimates use DHS birth data ($N \approx 2.3$ million) across more than 90,000 locations (*SI Appendix, Fig. S1*). *B* uses monthly ground station data for nearly 2,000 monitors ($N = 10,966$ station-months) in low- and middle-income countries (*SI Appendix, Fig. S5*). Upwind and downwind burned areas are based on monthly wind-direction vectors estimated from climate reanalyses data for each location-month (*Methods* for details). Histograms on the horizontal axis in panels *C* and *D* show, respectively, the distribution of baseline IMR and PM_{2.5}.

coefficients shows that we can reject the null of equality at the 10% level, but not at more stricter levels (*SI Appendix, Table S2*). Therefore, to further investigate the air pollution mechanism, we combine data on particulate pollution ($PM_{2.5}$) from nearly 2,000 available ground monitoring stations in low- and middle-income countries (*SI Appendix, Fig. S5*) with measures of upwind and downwind biomass burned area in the vicinity to construct a monthly panel spanning the period 2014 to 2018. Using these data, we estimate the relative impacts of upwind and downwind outdoor biomass burning on $PM_{2.5}$. We see a significant increase in $PM_{2.5}$ at ground station monitors due to upwind burned areas but find no effect of downwind burned areas (Fig. 2*B*). An additional square kilometer of area burned in the upwind direction increases $PM_{2.5}$ by $0.49 \mu\text{g}/\text{m}^3$ [95% CI 0.05 to 0.93]—an increase of 1% relative to the sample mean of $48.2 \mu\text{g}/\text{m}^3$ (Fig. 2*B*).

Similar to the patterns in infant mortality, upwind burning in a closer vicinity (within 30 km) has a much larger effect on $PM_{2.5}$, relative to burned areas at a further distance (*SI Appendix, Figs. S3B and S6*). These results suggest that changes in air quality are the plausible link between upwind burning and increased infant mortality.

The estimated effect of exposure to biomass burning on infant mortality remains robust to a variety of alternative models, including models in which differential trends and seasonal effects are allowed to vary subnationally across 1- or 2-degree grid cells (*SI Appendix, Table S2*) or models that exclude weather variables. Results are also unchanged with the exclusion or inclusion of child, mother, and household characteristics. These robustness tests suggest that our results are unlikely to be driven by household-level factors that may correlate with infant mortality and biomass burning exposure (*SI Appendix, Table S2*). Our main specification only considers the biomass burning that occurs in the upwind and downwind quadrants around the birth location. As an additional check, we also reestimate our main regression model with the inclusion of burned area, which is neither in the up nor downwind direction, and find that the estimated association with postbirth upwind exposure remains robust (*SI Appendix, Table S2, column 6*). The point estimate of 1.238 on upwind postbirth exposure is about 16.8% larger in magnitude than the point estimate in our main specification of 1.060. Accounting for non-up/downwind burned area potentially absorbs some of the noise in the upwind exposure coefficient resulting in a slight increase in the magnitude.

Finally, the estimates also remain robust to varying the radius used to calculate the exposure to biomass burning (*SI Appendix, Fig. S7A*). The magnitude of the upwind biomass burned area effect declines with an increase in the distance at which burning occurs. These results are strikingly similar to how the effect of upwind burning on $PM_{2.5}$ concentrations varies with distance (*SI Appendix, Fig. S7B*). These results do not contradict the reasoning that exposure to biomass burning affects infant mortality by increasing air pollution.

We find that prevailing levels of baseline infant mortality moderate the response to biomass burning exposure (Fig. 2*C* and *SI Appendix, Table S3*). An additional square kilometer of burned area has a relatively strong association with infant mortality in locations with low baseline mortality rates than in locations with high baseline infant mortality. This heterogeneity in the infant mortality response is consistent with previous evidence (23, 24). It is possible that exposure to smoke from biomass burning is a more prominent risk factor in areas where other risk factors to infant health, such as malaria, pose a lesser threat. While

we cannot directly test this hypothesis with the data we have, suggestive evidence that this may be the case is provided by an examination of the cross-country relationship between the share of infant deaths attributable to ambient air pollution and infant mortality rates (*SI Appendix, Fig. S18*). In a sample of 193 countries for which data are available over the 2003 to 2018 period, we see that the average share of infant deaths associated with pollution declines as the infant mortality rate increases.

Baseline ambient particulate pollution is negatively but not significantly related to the response of infant mortality to burned area exposure (Fig. 2*D* and *SI Appendix, Table S3*). We also find no evidence that household wealth helps mitigate the harmful effects of exposure to smoke from outdoor biomass burning (Fig. 2*E* and *SI Appendix, Table S3*). Both of these findings are again consistent with earlier evidence that found a linear (rather than concave) dose–response relationship between air pollution exposure and infant health at moderate $PM_{2.5}$ levels and found limited evidence for a moderating effect of household wealth (23).

To facilitate comparison of our estimates to estimates of pollution–infant mortality relationships from prior studies, we rescale the burned area–infant mortality relationship in Fig. 2*C* into $PM_{2.5}$ terms using the marginal effect of upwind burned area on $PM_{2.5}$ from Fig. 2*B*. Because coverage of ground $PM_{2.5}$ monitors is sparse, we estimate the average relationship between upwind burned area and $PM_{2.5}$ across all available ground monitors in our sample regions. On average, our estimates suggest that a 1 km^2 increase in upwind burned area leads to a $0.49 \mu\text{g}/\text{m}^3$ increase in $PM_{2.5}$ and results in 1.06 additional infant deaths. This rescaling implies that a $1 \mu\text{g}/\text{m}^3$ increase in $PM_{2.5}$ is associated with 2.16 additional infant deaths, on average. Combining our estimated differential effects of burning by baseline mortality rate with the distribution of baseline infant mortality rates across our sample, we find that our estimates correspond closely to the average effect sizes found in a range of studies across West Africa (24, 25), Sub-Saharan Africa (23), India (12), and China (26) (Fig. 3). At the lower end of the baseline mortality rate distribution, the effect size implied by our estimates is larger than that found in studies from Turkey (27) and Mexico City (28). However, only the Mexico City study, which was focused exclusively on a single large city, has confidence intervals that do not overlap with the estimates from our study.

We combine our estimates from the DHS sample with a harmonized infant mortality dataset from across low- and middle-income countries to estimate the annual number of infant deaths attributable to outdoor biomass fires in the 2004 to 2018 period. We define attributable deaths as infant deaths that would have been avoided if biomass burning was completely eliminated and calculate them as the difference between the number of model-predicted deaths under observed biomass burning conditions and under a hypothetical counterfactual scenario where outdoor biomass burned area was zero. Model results are based on estimates from Eq. 3, which accounts for the moderating effect of the prevailing baseline infant mortality rate shown in Fig. 2*C*. The statistical model is estimated on the DHS sample and then applied to the expanded sample of 105 low- and middle-income countries for which we were able to assemble district-level infant mortality data, limiting the sample in the expanded data to locations that are within the ranges of burned area and infant mortality observed in the DHS-based estimation sample (*SI Appendix, Fig. S8; Methods*). Collectively these countries account for 98% of global infant deaths in our sample period

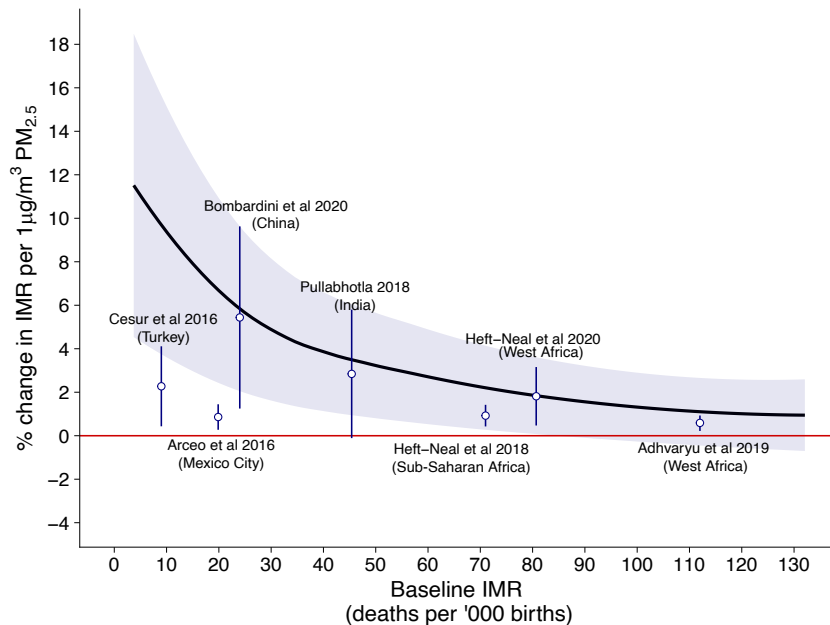


Fig. 3. Implied effect of $PM_{2.5}$ on infant mortality from this study compared to previous estimates. The black line with the 95% CI shaded region shows the percentage increase in IMR (relative to the baseline IMR) for a $1 \mu\text{g}/\text{m}^3$ increase in $PM_{2.5}$ from our study. These estimates are obtained by rescaling the biomass burning–infant mortality relationship in Fig. 2C into $PM_{2.5}$ terms using the marginal effect from Fig. 2B. The coefficient and 95% CI whiskers show estimates from previous studies.

and thus allow us to comprehensively assess the role of biomass burning as a determinant of infant mortality.

We find that, on average, eliminating exposure to smoke from biomass burning would have avoided nearly 5% of global infant deaths from 2004 to 2018. This share increases to more than a third in areas with high levels of exposure to outdoor biomass burning. Regions where this percentage is the highest include parts of Sub-Saharan Africa, areas around the Amazon basin in Brazil and equatorial South America, Southeast Asia, and parts of the North China plains (Fig. 4A).

The temporal patterns in infant mortality attributable to outdoor biomass burning exposure track observed changes in burned area. Average infant exposure to outdoor biomass burning increased somewhat in the initial years of the sample period until 2007, and then flattened or declined slightly through 2018 (Fig. 4B). The trend in estimated infant mortality attributable to biomass burning exposure (Fig. 4C) reflects this observed pattern in exposure and is relatively flat at around 1 additional death per '000 births across all sample years (Fig. 4C). While exposure to biomass burned area and infant mortality attributable to biomass burning exposure have remained relatively stable, the overall infant mortality rate globally has steadily declined (Fig. 4B), thanks in part to growing incomes and expanded access to health services and technologies. As other contributors to infant mortality have declined, we estimate that biomass burning-attributable infant deaths have increased as a share of total infant deaths (Fig. 4D), from 2.3% (95% CI 0.23 to 4.28) in 2004 to 3.6% (95% CI 0.74 to 6.50) in 2018.

We estimate that if biomass burning were eliminated entirely, countries across our sample would have experienced a reduction of nearly 130,000 infant deaths on average per year (95% CI 26,000 to 237,000). Countries in Africa would have seen the most significant gains in avoided infant deaths, with 98,000 avoided deaths on average per year (95% CI 15,000 to 183,000) (SI Appendix, Fig. S12), with an additional average decline per

year of 27,000 deaths in Asia and 4,600 in Latin America (Fig. 4E).

These estimates reflect a scenario in which biomass burning is brought down to zero. Because complete elimination in biomass burning may not be possible, we repeat the calculation using an alternate counterfactual scenario where outdoor biomass burned area in each location is held to the lowest observed level in any year for that location—a plausibly achievable reduction. The spatial pattern of infant deaths avoided under this achievable scenario is similar to that observed under the complete elimination scenario. The largest gains occur in Sub-Saharan Africa, where achievable reductions in burned area would have avoided more than 20% of overall infant deaths (SI Appendix, Fig. S9A). The trend in estimated infant mortality attributable to achievable reductions in burning remains around 0.6 additional deaths per '000 births across the 2004 to 2018 period (SI Appendix, Fig. S9B), while the share of overall infant deaths attributable to burning increases from 1.5% [95% CI (0.27, 2.87)] in 2004 to 2.1% [95% CI (0.51, 3.70)] in 2018 (SI Appendix, Fig. S9C). Under this reduction scenario, we estimate that 1.1 million infant deaths would have been avoided globally (70,000 per year) since 2004 (Fig. 4F and SI Appendix, Fig. S9D). This is roughly 60% of the estimated reduction in infant deaths under the complete elimination of biomass burning, suggesting that achievable biomass burning reductions could reduce the overall infant mortality burden by more than half.

We also calculate the contribution of recent trends in biomass burning to infant health outcomes by comparing differences in predicted mortality under observed trends versus under a setting where burning was fixed at baseline levels (computed as the 3-y average of location-specific burning over 2001 to 2003). We estimate that observed reductions in burning were associated with 147,000 fewer infant deaths in Africa and more than 2,000 fewer infant deaths in the Americas, relative to a world in which burning was fixed at 2001 to 2003 levels. On the other hand,

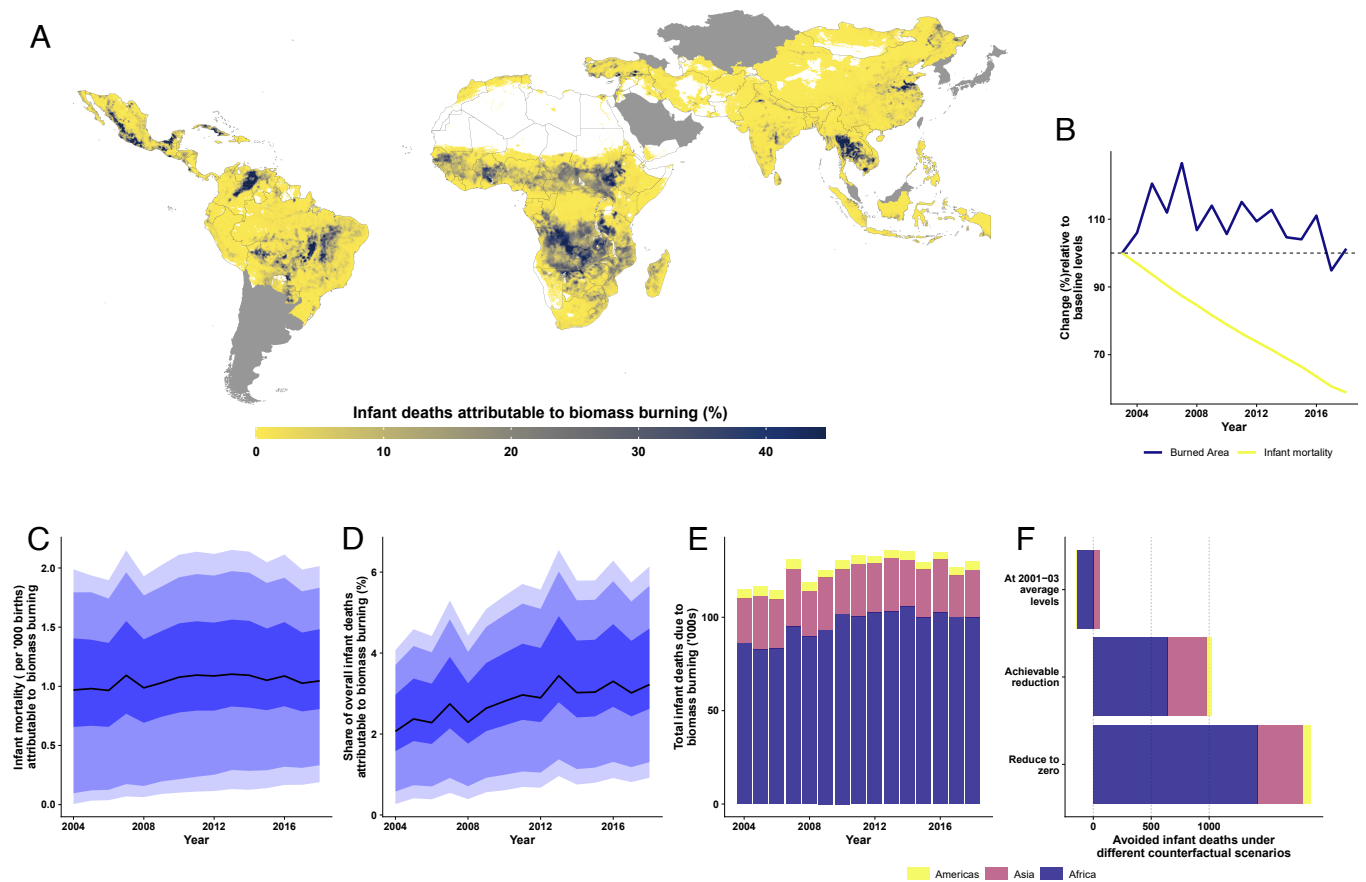


Fig. 4. Avoided infant deaths from eliminating postbirth exposure to outdoor biomass burning. (A) Average share of overall infant deaths avoided if biomass burning was reduced to zero over the period 2004 to 2018. (B) Births-weighted annual trends in infant mortality and burned area as a percentage of baseline levels (2003 infant mortality and 2001 to 2003 average burned area). (C–E), respectively, show the annual trends in (C) births-weighted infant mortality (deaths per '000 births) attributable to biomass burning exposure, (D) average infant mortality due to biomass burning exposure as share of overall infant mortality (%), and (E) number of avoided infant deaths in '000s by region that result from eliminating biomass burning. F shows the total avoided infant deaths (in '000s) under three different scenarios of biomass burning—holding burned area exposure at the baseline observed values, reduction to achievable levels, and complete elimination. The colors in the stacked bar charts in E and F show the break-up of the total infant deaths across three broad regions in the sample—Africa, Asia, and the Americas. The solid lines in C and D show the sample median, and the shaded regions show the 25th to 75th (darkest), 10th to 90th (medium), and 5th to 95th (lightest) percentile ranges based on bootstrapped estimates of predicted infant mortality values at each 1-km X 1-km grid cell, for each year.

because biomass burning in Asia increased over the study period, holding burning at baseline levels would have contributed to almost 61,000 fewer infant deaths in the region over the 2004 to 2018 period (Fig. 4F).

These regional differences result from the contrasting regional trends in biomass burning witnessed in recent years. Biomass burned area has declined substantially in the African region but experienced a modest increase across countries in Asia, relative to the baseline 2001 to 2003 period (SI Appendix, Fig. S10). In absolute terms, children in our African sample experienced a more than 20% reduction in average upwind burned area, from 4.75 km² per year in 2003 to 3.75 km² by 2018 (SI Appendix, Fig. S11A). During the same period, the infant mortality rate in Africa declined from 73 to 45 deaths per 1,000 births (SI Appendix, Fig. S11B), resulting in a reduction in annual all-cause infant deaths from 2.4 million in 2003 to 1.9 million in 2018 (SI Appendix, Fig. S11C). Despite a decline in exposure, the overall reduction in infant mortality implies that biomass burning contributes to an increasing share of infant mortality in Africa (SI Appendix, Fig. S12B). Annual infant deaths attributable to biomass burning exposure on the continent continue to remain at around 100,000 deaths per year throughout the sample period (SI Appendix, Fig. S12C). As a result, even though Africa experienced a substantial decrease in exposure compared to other regions, we estimate that

nearly 75% of global infant deaths due to burning still occur in Africa.

Discussion

The results of our study complement the limited existing evidence on the effects of biomass burning on overall mortality across all age groups and are broadly consistent with findings from studies focused on early childhood mortality. Quasi-experimental evidence using changes in wind direction similar to the research design in this study finds that agricultural fires contribute to all-cause mortality across all age groups in China (13), infant mortality in India (12), and stillbirth in Brazil (11). Our results help expand these regional estimates into a near-global picture of the role of biomass burning on child health.

Our results also help confirm findings from studies that use exposure based on chemical transport models (CTMs) combined with dose–response functions from literature to estimate premature deaths in both regional South-East Asia (29), Brazil (30), and Indonesia (31) and global settings (6, 21). Empirical confirmation of these model-based studies is important, as emissions inventories from biomass burning—a key input into CTM concentration estimates—can have high regional and temporal uncertainty and differ substantially across available

products (18, 32, 33), and because existing concentration–response (CR) relationships used to assess health impacts might not accurately capture the specific impact of pollutants emitted during biomass burning.

Our estimates are qualitatively similar to comparable findings from this CTM/CR work. For instance, from 2016 to 2019, removing anthropogenically set fires was estimated to avoid 265,000 global premature deaths annually among children under five (6)—a number comparable to our annual estimate of 130,000 deaths among individuals under the age of one. A previous study using cross-country DHS data similar to our estimation sample and relying on within-sibling comparison and CTM-based exposure estimated that over the 2000 to 2014 period, biomass fire exposure contributed to 9% of overall child (under-18) mortality in their sample of 55 low-income and middle-income countries (20). Our estimates suggest that biomass fires contribute to five percent of global infant mortality, broadly in agreement with these previous findings, but that contributions for infants are substantially higher in a large portion of low-income countries.

The effects that we find on infant mortality are also supported by growing evidence that exposure to smoke from fires results in adverse pregnancy and birth outcomes such as preterm birth, pregnancy loss (34) and low birth weights (11, 35–38). These adverse health impacts at birth could potentially result in a higher risk of infant mortality in the subsequent months. Our results are also consistent with evidence from studies that show exposure to smoke from large wildfires is associated with adverse birth outcomes and increased infant mortality—both in developed (39–41) as well as low-middle income countries (42–45). However, such fire events tend to result in short, extreme pollution episodes rather than widespread, repeated exposure to less extreme but unsafe levels of pollution that accompany the bulk of global biomass fires that are predominantly caused by seasonal human activities (46). Because prenatal pollution exposure has been linked to increased rates of stillbirths (34, 47–50) and our sample is limited to live-born children, pregnancy mortality–related selection may downward bias our estimated impacts of prenatal burning on infant mortality and contribute to the noisier estimates we find for prebirth, relative to postbirth, exposure periods (*SI Appendix, Fig. S3*).

Our findings on spatial heterogeneity in the contribution of biomass burning to infant mortality also help corroborate the regional distribution of mortality estimates found in earlier studies. We find that the contribution of outdoor biomass fires to the overall infant mortality rate is exceptionally high in some low-income locations such as Sub-Saharan Africa, but also high in somewhat higher-income locations with relatively lower overall infant mortality but which are experiencing increasing fires—for instance, in Thailand, Laos, Cambodia, and other areas of Southeast Asia (Fig. 4A) (51). These patterns echo results from previous studies that also suggest that many parts of Sub-Saharan Africa and Southeast Asia are particularly at risk of high fire-attributable mortality (6, 20, 21). Though the model used in Fig. 4A incorporates the variation in both burned area and baseline infant mortality rate, the spatial patterns we observe are predominantly driven by the variation in burning. Excluding the mediating effect of baseline infant mortality results in a very similar spatial distribution of impacts that result from our main model (*SI Appendix, Fig. S15A*). The share of infant deaths attributable to burning is 2.16 percentage points higher when baseline infant mortality is not included in the model, rising to 16 percentage points in locations with high levels of burning and high baseline IMR (*SI Appendix, Fig. S15B*).

While particulate matter exposure is a known driver of poor infant health outcomes, the extent to which biomass burning drives these effects is not clear. To assess biomass's contributions to total PM_{2.5} impacts, we combine our estimates of biomass-burning-attributable infant deaths with estimates from the Global Burden of Disease (GBD) (52) on attributable infant deaths from all PM_{2.5} sources to estimate the share of overall PM_{2.5} deaths attributable to biomass burning. We calculate that biomass fires contribute an average of 15.4% of total PM infant deaths at the country level over the 2004 to 2018 period (*SI Appendix, Fig. S13A*). Globally, while PM_{2.5}-related infant deaths have been declining, infant deaths due to biomass fires have been on the rise (*SI Appendix, Fig. S13B*). As a result, again based on GBD estimates of total infant deaths attributable to all PM_{2.5} pollution, we calculate that the contribution of biomass fires to overall PM-related infant deaths has risen from 11% in 2004 to over 21% by 2018 (*SI Appendix, Fig. S13C*).

Our results additionally suggest that the negative health impacts of biomass burning likely dominate any potential health benefits associated with economic activity that generates the anthropogenic biomass fires. The coefficient on the downwind burned area which captures the potential local economic benefits of burning is close to zero (Fig. 2C). We therefore focus on the upwind burning coefficient alone rather than following previous studies that report the difference between upwind and downwind coefficients (11). In cross-sectional analysis, we also do not find any evidence that households that are located in places with high burned areas are wealthier (*SI Appendix, Fig. S14*). Consistent with other recent empirical studies (11–13), we find that the health impacts of biomass burning are concentrated within relatively close proximity to the burning itself. This suggests that jurisdictions that undertake policies to reduce burning within a locality will likely also be the primary beneficiaries of that policy in terms of health improvements. This stands in contrast to perhaps more challenging policy settings such as large wildfires or Saharan dust, in which transboundary movement of pollutants is a substantial source of health impacts (24, 25, 42).

Finally, global fire model simulations project an increase in fire activity and burned area in the near future due to human activities and temperature-driven increases linked to climate change (53, 54). These projected increases have the potential to reverse the decline in burned area observed in recent years. Our results suggest that such increases in burned areas would accelerate the contribution of outdoor biomass fire exposure to air pollution-related infant deaths and worsen overall infant mortality. Policies to mitigate anthropogenic fire activity, therefore, offer great promise for improving global health outcomes.

Materials and Methods

Data.

Infant mortality data. Data on infant mortality outcomes used in the estimation sample are drawn from birth data in the Demographic and Health Surveys (DHS). The DHS are nationally representative surveys conducted in many low- and middle-income countries worldwide. Surveyed households are selected using a two-stage sampling procedure. DHS first selects enumeration areas (or clusters), usually drawn from the most recent population census. Within each enumeration cluster, DHS then selects a random set of survey participants based on a listing of all households within the sample enumeration area. The survey interviews all women aged 15 to 49 in the selected households (55). In addition to a number of health-related information, for each woman interviewed, the DHS records their complete birth histories, including the month and year of birth for each child ever-born, the mortality outcome for each birth, and the age of death if the child has not survived. The DHS also provides the geographic coordinates

for the primary enumeration sample cluster for most survey rounds. To preserve respondent anonymity, the location of the DHS clusters in the public data release is displaced in a random distance and direction, with urban locations displaced by 0 to 2 km, while rural locations are displaced by 0 to 5 km (with 1% of the locations displaced by 0 to 10 km) (56). This displacement could lead to potential measurement error, which we discuss in more detail in the section on Measurement Error below.

We construct a monthly time series of births recorded at each cluster location using these recalled birth history data and location information. Our primary outcome variable is a binary indicator taking the value one if the child was reported to have died within 12 mo after birth. We use data on the births recorded in all available DHS rounds occurring between 2004 and 2018 (SI Appendix, Table S1). Our final sample consists of 2,237,307 births, and the mean sample infant mortality rate is 53 deaths per 1,000 births.

In addition to the DHS birth data used in the estimation, we also construct a harmonized dataset of subnational infant mortality rates to calculate the number of attributable deaths due to fire smoke globally. To generate the IMR estimates, we utilize a gridded data product published by the IHME (Institute for Health Metrics and Evaluation) in a 2019 study (57, 58), with IMR estimates at a 5 km × 5 km spatial resolution, and estimates and vital statistics of countries not in the IHME product (59–61). The IHME product does not cover all the countries in our prediction sample due to several reasons. For example, the list excludes Brazil and Mexico due to the availability of vital statistics, and China and Turkey due to middle-high SDI (Socio-Demographic Index) score (57). To generate the estimates for the countries not included in the IHME product, we utilize vital statistics for Turkey (60), Mexico (59), state-level IHME estimates for India (58), 2017 GBD study estimates for Brazil (62), and a study on child mortality in China (61). For Brazil and China estimates, we could obtain only under-5 mortality estimates. To generate the IMR estimates, we calculate the national-level ratio of IMR-to-Under-5 mortality and scale down the Under-5 mortality estimates for each unit (counties for China and states for Brazil) by multiplying the mortality estimate by the ratio. Finally, not all datasets cover the full extent of the study period. As a result, we extrapolate the estimates where necessary to generate the IMR estimates for the missing years. To utilize the study estimates of IMR effects in calculating the attributable number of deaths globally, we need an inclusion criterion that ensures the extended sample fall within the distribution of the observed range of infant mortality rates observed in the DHS estimation sample. The out-of-sample country is included in our prediction sample if 90% or more of its IMR estimates fall within the fifth and 95th percentiles of our estimation sample countries' estimates.

We use these data to construct a panel of yearly infant mortality rates at a 5-km grid-cell level. We combine these data with estimates of the annual number of births within each grid cell constructed from WorldPop (63), and the annual outdoor biomass burned area. We also limit our counterfactual scenario estimates to countries that have ranges of burned area and infant mortality within the supports of our DHS-based estimation sample (SI Appendix, Fig. S8). Of note, 105 countries met both of these criteria and were included in our analysis. Collectively, these 105 countries account for 98% of total infant deaths during our study period. To construct the annual births country-level totals, we first utilized the WorldPop's 2015 gridded data product to assign each grid a percentage of total births that occurred in the country that the cell falls into. After obtaining the percentage, we then utilized a country-level world births UN dataset to compute the number of annual births for the year falling within the study period (2003 to 2018), by multiplying the percentage of total births that occurred in country according to WorldPop 2015 gridded estimates by the total births in that year.

Burned area data. We estimate exposure to outdoor biomass burning using burned area data from the European Space Agency Climate Change Initiative fire data product. Specifically, we use the LTDR Fire_cci version 1.1 pixel product (FireCCILT11) on monthly global burned area. FireCCILT11 provides burned area data at 0.05-degree (≈ 5 km) spatial resolution based on Advanced Very High Resolution Radiometer (AVHRR) imagery (64–66). Validation studies show that FireCCILT11 provides consistent and accurate estimates of burned area over a long time period (67). We also find good agreement in the overall and regional trends observed using the FireCCILT11 with other sources of burned area over the study period. Each birth in our estimation sample, on average,

is exposed to 11.5 km² of outdoor biomass burned area per month during pregnancy and in the 12 mo after birth (within a 30-km radius around the birth location). Recently, products incorporating small fires show more burned area than previous products, but the general spatial distribution across products is found to be similar (68). If locations with a higher burned area in our sample are also likely to have more small fires, then our estimates reflect the overall impact of both small and large fires. Empirically, we are also constrained by the limited temporal and spatial coverage of burned area products that account for small fires.

Weather data. Monthly data on precipitation, temperature, wind direction, and wind speed come from the fifth generation of European ReAnalysis (ERA5) data. ERA5 data provide global climate reanalysis variables at a 30-km grid, at three hourly intervals (69). The data were downloaded from the Copernicus Climate Change Service (C3S) Climate Data Store. We use the aggregated monthly products and extract the weather variables at the location of each birth for the prebirth and postbirth months.

Construction of biomass burning exposure. Using the wind direction at the location of each birth, we identify upwind and downwind quadrants for each month during pregnancy and in the 12 mo after birth. The “upwind” quadrant refers to the direction from which wind is blowing to the birth location, while the “downwind” quadrant is where the wind is blowing away from the birth location (SI Appendix, Fig. S2). We then calculate the outdoor biomass burned area in the upwind and downwind quadrants. Our assignment of upwind and downwind quadrants is based on the average horizontal (*u*) and vertical (*v*) components of the wind vector for each month. The use of the monthly average could lead to potential measurement error if the average masks significant within-month wind direction variability. We assess the extent to which wind direction misclassification could influence our results in the Measurement Error section below.

Our main estimates use burned areas within a 30-km radius around the birth location. Results from using burned areas within other distances are shown in the robustness tests. Using the 30-km radius, we estimate an average upwind burned area of 2.9 km² per month and an almost similar amount of 2.8 km² of downwind burned area. On average, upwind burned area forms about 25% of the total burned area in the births regression sample. To ease data processing, we use this proportion to approximate the amount of upwind burned area exposure around the grid cells in the extended sample. We calculate the total burned area around each grid cell and assign one-fourth of this to be in the upwind direction.

Air pollution ground station monitoring data. Data on monthly particulate matter pollution (*PM*_{2.5}) measured at ground station monitors are drawn from daily recorded *PM*_{2.5} measurements collected by monitors in the openAQ database (<https://openaq.org>). We subset the data to stations located in low- and middle-income countries as these are more likely to reflect pollution sources and pollution levels that represent the births sample used in our estimates. Our final sample consists of 2040 monitors (SI Appendix, Fig. S5A) and has an average monthly *PM*_{2.5} of 48.2 μg/m³. Similar to the birth data, we extract monthly weather variables and calculate upwind and downwind burned areas at each ground station monitor using ERA5 and FireCCILT11 data.

Empirical methods. We use the following regression model to estimate the relationship between burned area exposure on infant mortality:

$$y_{i,c,g,m,y} = \sum_d \beta_{1,d} BA_{up,d,i,c,m,y}^{pre} + \sum_d \beta_{2,d} BA_{up,d,i,c,m,y}^{post} + \sum_d \beta_{3,d} BA_{down,d,i,c,m,y}^{pre} + \sum_d \beta_{4,d} BA_{down,d,i,c,m,y}^{post} + \delta X_{i,c,g,m,y} + \mu_c + \lambda_{g,m} + \delta_{g,y} + \varepsilon_{i,c,g,m,y} \quad [1]$$

where the outcome variable is an indicator for birth *i*, in cluster *c* located within country *g*, occurring in month *m* and year *y* resulting in a death within 12 mo of birth. *BA*^{pre} and *BA*^{post} are, respectively, burned area (in km²) for the 9 mo before and 12 mo after birth (including month of birth). The subscripts *up*, *d* and *down*, *d* refer, respectively, to the burned area in upwind and downwind directions in distance bins *d* around cluster *c* corresponding to each birth. We use burned area within 0 to 30, 30 to 40, and 40 to 50-km radii around each

cluster to flexibly allow for burned area effect to vary by distance. Upwind and downwind exposure refers to the outdoor biomass burned areas in the upwind and downwind quadrants (SI Appendix, Fig. S2), measured as the average monthly burned area in square kilometers during prebirth and postbirth periods. We include a set of individual and household characteristics $\mathbf{X}_{i,c,g,m,y}$ such as child gender and birth order, age, and education of the mother, as well as weather variables (quadratic polynomials of temperature, precipitation, and wind speed, and wind direction). Our regression include μ_c , $\lambda_{g,m}$, and δ_y , respectively, DHS cluster, country by birth month and country by year of birth fixed effects. We weight observations by the product of survey-specific household survey weights (supplied by DHS) and country population weights in order to generate estimates that are representative of the 54 countries across our sample (23, 70). We cluster the standard errors at 1-degree grid cell level to account for potential spatial correlation in biomass burning. Our results show that prebirth exposure is not substantially associated with mortality risk, but postbirth exposure to biomass burned area within the 0 to 30 km in the upwind direction is. (SI Appendix, Fig. S3).

Using a similar regression model, we estimate the impact of upwind and downwind burned areas on monthly particulate pollution $PM_{2.5}$ measured at ground station monitors located in low- and middle-income countries.

$$PM_{2.5}_{i,t} = \sum_d \beta_{1,d} BA_{up,i,t} + \sum_d \beta_{2,d} BA_{down,i,t} + \delta \mathbf{X}_{i,t} + \mu_i + \lambda_t + \nu_{i,t}. \quad [2]$$

The outcome here is monthly average $PM_{2.5}$ in micrograms per cubic meter at ground station monitor i in month-year t . We calculate the monthly burned area around each ground station monitor in upwind and downwind directions within the same distance bins as we use in the infant mortality regression in Eq. 1. We estimate the effect of outdoor biomass burning on particulate pollution using a fixed effects regression model with location and month fixed effects μ_i and λ_t , respectively. These fixed effects account for any unobserved, time-invariant factors specific to monitor locations, and shocks common to each month. We also include a vector of weather controls (precipitation, temperature, and wind variables) to account for local climatic conditions that may be correlated with $PM_{2.5}$ at the ground stations. Similar to the infant mortality effect, we find that burned area within the 0 to 30 km in the upwind direction increases $PM_{2.5}$ levels (SI Appendix, Fig. S6).

Because the relationship between burned area and $PM_{2.5}$ is heterogeneous over space, we would ideally estimate this relationship separately for each location. However, because coverage of ground monitors in developing countries is sparse (SI Appendix, Fig. S5A), we do not have sufficient data to estimate region-specific relationships. Instead, we resort to a global average to approximate local relationships. Our average estimated burned area - $PM_{2.5}$ relationship will reflect the spatial distribution of monitors and is therefore likely to be more representative in areas with better ground monitor coverage (eg, South Asia) and less representative in areas with poor ground monitor coverage (eg, Africa).

We also examine the sensitivity of the infant mortality and particulate pollution regressions to the radius used to compute burned area radius. Our central estimates use a 30-km radius to define nearby burning. We vary this radius in 5-km increments from 25 to 40 km for infant mortality and the pollution model (SI Appendix, Fig. S7). Overall, the point estimates remain stable across the definitions of nearby burning, with a slight decrease in magnitude as we increase the radius. The coefficient point estimates become less precise as the exposure distance becomes too narrow or wide. Using a smaller radius (0 to 25 km) reduces the sample exposure measure's variation, increasing the standard errors. On the other hand, as the exposure buffer widens (0 to 40 km), we increase the likelihood of measurement error in the upwind exposure, which attenuates the point estimates and reduces precision.

The key takeaway is that we observe a similar diminishing effect of burning with distance for pollution and infant mortality models (SI Appendix, Fig. S7). The remarkably identical pattern we observe for both outcomes lends further support to pollution being the primary mechanism through which outdoor biomass burning affects infant mortality: Burning that occurs further away has less impact on particulate air pollution and, therefore, has a smaller effect on health.

To estimate the moderating role of baseline infant mortality, ambient baseline $PM_{2.5}$, or wealth levels, we interact linear postbirth exposure within 0 to 30 km with the respective variables:

$$y_{i,c,g,m,y} = \alpha_1 BA_{up,0-30,i,c,m,y}^{post} + \alpha_2 (BA_{up,0-30,i,c,m,y}^{post} \times Z_i) + \alpha_3 BA_{down,0-30,i,c,m,y}^{post} + \alpha_4 (BA_{down,0-30,i,c,m,y}^{post} \times Z_i) + \delta \mathbf{X}_{i,c,g,m,y} + \mu_c + \lambda_{g,m} + \delta_y + \nu_{i,c,g,m,y}, \quad [3]$$

where Z_i is the baseline infant mortality (IMR), ambient baseline $PM_{2.5}$, or wealth levels. Baseline IMR is constructed as follows: We take the sample infant mortality rate for the year prior to birth averaged over clusters located within 1-degree grid cells around each birth location. Baseline $PM_{2.5}$ is similarly constructed as the lagged average $PM_{2.5}$ at 1-degree grid-cells around each birth location. In the case of wealth level, Z_i is a vector of dummy variables for wealth quintile. We see no significant variation in the impact of burned area across household wealth or baseline pollution levels. However, the impact of upwind burning exposure reduces with an increase in baseline infant mortality (SI Appendix, Table S4).

Measurement error. Our exposure variables (upwind burned area) potentially contain some measurement error which could influence our regression estimates. We detail three key measurement error concerns in our context.

First, the DHS data record the respondent's current location but not where she was residing when gestation or early-life exposure to pollution could have occurred. To evaluate the extent to which our results are affected by this measurement error, we reestimate our main specification limiting the sample to births whose mothers had resided in the current (survey) location since before the birth occurred. To do so, we utilize information from a subset of DHS surveys that ask how long the respondent (the mother) has resided in the current location. This question is available for only 68 of the 118 DHS surveys we use in our analysis. We reestimate our main specification for all the births in these 68 surveys and then run our regression using only the births that have occurred since the respondent has resided in the current survey location. The sample size reduces by about 11% when we restrict the births to those that happened in the current location. However, the coefficient on upwind burned area exposure remains very similar across these two samples: 1.375 for all the births in the 68 surveys versus 1.183 for the sample restricted to the current location (SI Appendix, Table S3). The coefficient for all births is 16.2% larger than the coefficient obtained when the sample is restricted to births occurring in the current location, but the two estimates are not statistically different. We also note that the coefficient in the restricted sample is less precise and significant only at a 10% level. This evaluation exercise suggests that the measurement error in the mother's location at the time of birth is unlikely to affect our results severely. However, we cannot rule out additional measurement errors that might arise due to women moving to a different location (their paternal home, for instance) to give birth and returning to their current location after delivery.

Second, as noted earlier, the cluster geographic coordinates are randomly displaced in the publicly released DHS data to preserve respondent anonymity. As a result of this displacement, the amount burned area around a birth location may contain measurement error. We look at existing evidence to assess the degree to which this locational error may affect our results and undertake a simulation exercise within our study context. A previous study quantifying the extent of bias that can arise in regression estimates due to the spatial location error in DHS data found that using a neighborhood buffer to extract environmental exposure variables minimizes bias (71). For relatively smooth continuous raster data (as is the case with the burned area data we use), their analysis suggests that using a 5-km buffer around both urban and rural clusters alleviates the bias in regression estimates to a considerable extent (pp. 30). Our research design relies on a 30-km radius to measure exposure to burned area—well over the 5-km buffer suggested by ref. 71. The muted impact of the DHS cluster location errors on our estimates is also supported by the results of our simulation exercise, described below.

The simulation exercise we undertake starts by creating a burned area raster data mimicking the actual data we use (SI Appendix, Fig. S15A). This raster uses the same resolution as our actual data, with a similar degree of spatial autocorrelation of 0.2. In each simulation run, we start by generating 100 random points on the burned area raster to represent DHS clusters

(SI Appendix, Fig. S15A). We calculate the upwind burned area based on the “true” location and generate the outcome variable for each location using a “true” effect size of 0.5 plus an additive normally distributed error term:

$$y_i^{true} = \beta^{true} upwindBA_i^{true} + U, \quad U \sim \mathcal{N}(0, 1). \quad [4]$$

We then displace these points by randomly jittering them and calculate the burned area measured with error using these jittered locations (SI Appendix, Fig. S15B). We then run a regression model using the mismeasured burned area and compare the coefficient estimate we obtain to β^{true} , the true effect.

We also assess the role of a third source of measurement error via our simulation exercise: misclassification of upwind direction. Our analysis uses monthly average wind direction to assign upwind and downwind quadrants for each location-month observation in our sample. Upwind assignment based on monthly averages could result in measurement error if the monthly average masks a significant degree of daily variation in wind direction. We assess the extent of disagreement between monthly versus daily wind measures using two samples of hundred randomly selected DHS locations for two arbitrary months of the sample. The upwind quadrant based on the monthly average differs from the upwind categorization based on modal daily wind direction in 12 to 14% of the observations in these two samples (SI Appendix, Fig. S15C). We incorporate the potential misclassification in the upwind direction in our simulation by assigning the burned area from the wrong quadrant to a subset of the locations. For simplicity, we use the northeast quadrant as the “true” upwind area in our simulation. In contrast, locations with misclassified wind direction received burned area exposure based on the southeast quadrant.

We vary the random displacement in DHS locations from 0 to 10 kilometers in increments of 2 km and the proportion of clusters with misclassified wind direction from 2 to 20% in increments of 2%. For each combination of displacement and proportion with misclassified wind direction, we ran the simulation 100 times each. Our results suggest that, at the extreme, if with a random displacement of DHS clusters by 10 km and 20% of them having misassigned wind direction, the exposure to upwind burned area would contain a measurement error of 1% (SI Appendix, Fig. S15D). As a result of this measurement error, the regression coefficient could be biased up to 5.6% from the true effect (SI Appendix, Fig. S15E).

Infant mortality attributable to biomass burning globally. Our model linking infant mortality to nearby burned area is estimated on the sample of observed births in the DHS. In order to better understand the global implications of biomass burning on infant health, we apply the estimated relationships to the broader sample of 105 countries available in our extended sample at 5-km grid cell level. We derive infant mortality due to burning under three different scenarios where the counterfactual burned area BA_{ct}^{cf} for each grid cell c and year t is defined as follows: scenario i) $BA_{ct}^{cf} = 0$, i.e., burned area is eliminated completely, scenario ii) $BA_{ct}^{cf} = BA_{c0}$, i.e., burned area is fixed at the observed baseline value (the 3-year average from 2001 to 2003), and scenario iii) $BA_{ct}^{cf} = \min(BA_{ct})$, $2004 < t < 2018$, for each grid cell c , i.e., burned area is reduced to the minimum observed within each grid cell during the sample period. We refer to this minimum burned area as a plausibly achievable counterfactual scenario. The observed minimum is zero in many regions of the world but remains fairly high in locations that experience heavy burning each year—for example, central and

southern Africa (SI Appendix, Fig. S17). We note that it is difficult to know how realistic these achievable reductions are in practice. But given the limitations of the data and existing evidence on the drivers of burned area, these observed minimum values serve as an approximation. For each scenario, we calculate ΔIMR_{ct} , the change in IMR for each year in each grid cell owing to changes in the burned area. We start by estimating the counterfactual change in burned area ΔBA_{ct} for each grid cell-year:

$$\Delta BA_{ct} = BA_{ct} - BA_{ct}^{cf}, \quad [5]$$

where BA_{ct} is the observed burned area and BA_{ct}^{cf} is the counterfactual burned area corresponding to each scenario. We then apply the estimated parameters from the regression in Eq. 3, the coefficients on upwind postbirth exposure (α_1) and its interaction with baseline infant mortality (α_2), to estimate the change in infant mortality. While doing this, we ensure that the prevailing infant mortality rate (IMR_{ct-1}) we use reflects the evolution of infant mortality corresponding to the counterfactual scenario in the preceding year. We start by initializing infant mortality rate to IMR_{c0} , the baseline grid cell-level IMR ($t = 0$ corresponds to 2003 in our study period). The attributable change in infant mortality at $t = 1$ is:

$$\Delta IMR_{ct} = \alpha_1 \Delta BA_{ct} + \alpha_2 \Delta BA_{ct} * IMR_{ct-1}. \quad [6]$$

We then update the measure of prevailing IMR to account for the estimated change in infant mortality (ΔIMR_{ct}) under the counterfactual. This updated IMR (IMR_{ct}^{new}) is given by:

$$IMR_{ct}^{new} = \Delta IMR_{ct} + IMR_{ct-1}. \quad [7]$$

Using the updated IMR, we estimate the change in infant mortality for the next year under the counterfactual change in burned area:

$$\Delta IMR_{ct} = \alpha_1 \Delta BA_{ct} + \alpha_2 \Delta BA_{ct} * IMR_{ct-1}^{new}. \quad [8]$$

We repeat this process until the last year in our sample (2018) giving us a time series of ΔIMR_{ct} for each grid cell location. We iterate over bootstrapped parameter estimates α_1 and α_2 in Eq. 3 in order to derive confidence intervals for the location-specific predictions ΔIMR_{ct} . Using the observed infant mortality rate and ΔIMR_{ct} , we calculate the share of total infant mortality (S_{ct}) attributable to biomass burning exposure:

$$S_{ct} = \frac{\Delta IMR_{ct}}{IMR_{ct}}. \quad [9]$$

Finally, we estimate the number of infant deaths attributable to biomass burning exposure in each location (ID_{ct}):

$$ID_{ct} = \Delta IMR_{ct} \times b_{ct}, \quad [10]$$

where b_{ct} is number of births at location c for year t from WorldPop. For each year, we sum ID_{ct} across all locations to calculate the total number of attributable infant deaths across our extended sample of 105 countries.

Data, Materials, and Software Availability. Anonymized data and code have been deposited in Zenodo (<https://doi.org/10.5281/zenodo.7854094>) (72).

1. E. Chuvieco *et al.*, Human and climate drivers of global biomass burning variability. *Sci. Total Environ.* **779**, 146361 (2021).
2. E. Chuvieco *et al.*, Historical background and current developments for mapping burned area from satellite earth observation. *Remote Sens. Environ.* **225**, 45–64 (2019).
3. S. Akagi *et al.*, Emission factors for open and domestic biomass burning for use in atmospheric models. *Atmos. Chem. Phys.* **11**, 4039–4072 (2011).
4. J. S. Levine, *Biomass Burning and Global Change: Remote Sensing, Modeling and Inventory Development, and Biomass Burning in Africa* (MIT Press, 1996), vol. 1.
5. I. Colbeck, M. Lazaridis, Aerosols and environmental pollution. *Naturwissenschaften* **97**, 117–131 (2010).
6. G. Roberts, M. Wooster, Global impact of landscape fire emissions on surface level pm2.5 concentrations, air quality exposure and population mortality. *Atmos. Environ.* **252**, 118210 (2021).
7. L. Giglio, J. T. Randerson, G. R. van der Werf, Analysis of daily, monthly, and annual burned area using the fourth-generation global fire emissions database (GFED4). *J. Geophys. Res.: Biogeosci.* **118**, 317–328 (2013).
8. M. Zubkova, L. Boschetti, J. T. Abatzoglou, L. Giglio, Changes in fire activity in Africa from 2002 to 2016 and their potential drivers. *Geophys. Res. Lett.* **46**, 7643–7653 (2019).
9. C. Lauk, K. H. Erb, Biomass consumed in anthropogenic vegetation fires: Global patterns and processes. *Ecol. Econ.* **69**, 301–309 (2009).
10. J. T. Abatzoglou, A. P. Williams, Impact of anthropogenic climate change on wildfire across western US forests. *Proc. Natl. Acad. Sci. U.S.A.* **113**, 11770–11775 (2016).
11. M. A. Rangel, T. S. Vogl, Agricultural fires and health at birth. *Rev. Econ. Stat.* **101**, 616–630 (2019).
12. H. K. Pullabhotla, PhD thesis (University of Illinois at Urbana-Champaign, 2019).
13. G. He, T. Liu, M. Zhou, Straw burning, pm2.5, and death: Evidence from China. *J. Dev. Econ.* **145**, 102468 (2020).
14. P. Singh, S. Dey, Crop burning and forest fires: Long-term effect on adolescent height in India. *Res. Energy Econ.* **65**, 101244 (2021).
15. J. Chen *et al.*, A review of biomass burning: Emissions and impacts on air quality, health and climate in China. *Sci. Total Environ.* **579**, 1000–1034 (2017).
16. V. Samburova *et al.*, Polycyclic aromatic hydrocarbons in biomass-burning emissions and their contribution to light absorption and aerosol toxicity. *Sci. Total Environ.* **568**, 391–401 (2016).
17. G. Lammel, A. Heil, I. Stemmler, A. Dvorská, J. Klánová, On the contribution of biomass burning to POPs (PAHs and PCDDs) in air in Africa. *Environ. Sci. Technol.* **47**, 11616–11624 (2013).
18. X. Pan *et al.*, Six global biomass burning emission datasets: Intercomparison and application in one global aerosol model. *Atmos. Chem. Phys.* **20**, 969–994 (2020).

19. A. L. Johnson, M. J. Abramson, M. Dennekamp, G. J. Williamson, Y. Guo, Particulate matter modelling techniques for epidemiological studies of open biomass fire smoke exposure: A review. *Air Quality, Atmos. Health* **13**, 35–75 (2020).
20. T. Xue *et al.*, Associations between exposure to landscape fire smoke and child mortality in low-income and middle-income countries: A matched case-control study. *Lancet Planet. Health* **5**, e588–e598 (2021).
21. F. H. Johnston *et al.*, Estimated global mortality attributable to smoke from landscape fires. *Environ. Health Perspect.* **120**, 695–701 (2012).
22. D. J. P. Barker *et al.*, *The Window of Opportunity: Pre-pregnancy to 24 Months of Age* (Karger Medical and Scientific Publishers, 2008), vol. 61.
23. S. Heft-Neal, J. Burney, E. Bendavid, M. Burke, Robust relationship between air quality and infant mortality in Africa. *Nature* **559**, 254–258 (2018).
24. S. Heft-Neal, J. Burney, E. Bendavid, K. K. Voss, M. Burke, Dust pollution from the Sahara and African infant mortality. *Nat. Sustain.* **3**, 863–871 (2020).
25. A. Adhvaryu, P. Bharadwaj, J. Fenske, A. Nyshadham, R. Stanley, "Dust and death: Evidence from the West African Harmattan" (National Bureau of Economic Research Technical Report, 2019).
26. M. Bombardini, B. Li, Trade, pollution and mortality in China. *J. Int. Econ.* **125**, 103321 (2020).
27. R. Cesur, E. Tekin, A. Ulker, Air pollution and infant mortality: Evidence from the expansion of natural gas infrastructure. *Econ. J.* **127**, 330–362 (2017).
28. E. Arceo, R. Hanna, P. Oliva, Does the effect of pollution on infant mortality differ between developing and developed countries? Evidence from Mexico City. *Econ. J.* **126**, 257–280 (2016).
29. C. L. Reddington *et al.*, Air pollution from forest and vegetation fires in southeast Asia disproportionately impacts the poor. *GeoHealth* **5**, e2021GH000418 (2021).
30. M. Nawaz, D. Henze, Premature deaths in Brazil associated with long-term exposure to pm2.5 from Amazon fires between 2016 and 2019. *GeoHealth* **4**, e2020GH000268 (2020).
31. L. Kiely *et al.*, Air quality and health impacts of vegetation and peat fires in equatorial Asia during 2004–2015. *Environ. Res. Lett.* **15**, 094054 (2020).
32. Y. Shi, T. Matsunaga, M. Saito, Y. Yamaguchi, X. Chen, Comparison of global inventories of CO₂ emissions from biomass burning during 2002–2011 derived from multiple satellite products. *Environ. Poll.* **206**, 479–487 (2015).
33. T. Liu *et al.*, Diagnosing spatial biases and uncertainties in global fire emissions inventories: Indonesia as regional case study. *Remote Sens. Environ.* **237**, 111557 (2020).
34. T. Xue *et al.*, Open fire exposure increases the risk of pregnancy loss in south Asia. *Nat. Commun.* **12**, 1–10 (2021).
35. A. M. C. da Silva, G. P. Moi, I. E. Mattos, S. d. S. Hacon, Low birth weight at term and the presence of fine particulate matter and carbon monoxide in the Brazilian Amazon: A population-based retrospective cohort study. *BMC Pregnancy Childbirth* **14**, 1–8 (2014).
36. P. Mouganie, R. Ajeeb, M. Hoekstra, Evidence from government failure in Lebanon. The effect of open-air waste burning on infant health (2020).
37. B. A. Jones, R. P. Berrens, Prescribed burns, smoke exposure, and infant health. *Contemp. Econ. Policy* **39**, 292–309 (2021).
38. J. Li *et al.*, Exposure to landscape fire smoke reduced birthweight in low- and middle-income countries: Findings from a siblings-matched case-control study. *eLife* **10**, e69298 (2021).
39. S. M. Holm, M. D. Miller, J. R. Balmes, Health effects of wildfire smoke in children and public health tools: A narrative review. *J. Expos. Sci. Environ. Epidemiol.* **31**, 1–20 (2021).
40. S. Heft-Neal, A. Driscoll, W. Yang, G. Shaw, M. Burke, Associations between wildfire smoke exposure during pregnancy and risk of preterm birth in California. *Environ. Res.* **203**, 111872 (2022).
41. M. Abdo *et al.*, Impact of wildfire smoke on adverse pregnancy outcomes in Colorado, 2007–2015. *Int. J. Environ. Res. Public Health* **16**, 3720 (2019).
42. N. Sastry, Forest fires, air pollution, and mortality in southeast Asia. *Demography* **39**, 1–23 (2002).
43. S. Jayachandran, Air quality and early-life mortality evidence from Indonesia's wildfires. *J. Hum. Res.* **44**, 916–954 (2009).
44. J. S. Tan-Soo, S. K. Pattanayak, Seeking natural capital projects: Forest fires, haze, and early-life exposure in Indonesia. *Proc. Natl. Acad. Sci. U.S.A.* **116**, 5239–5245 (2019).
45. E. Frankenberg, D. McKee, D. Thomas, Health consequences of forest fires in Indonesia. *Demography* **42**, 109–129 (2005).
46. N. Andela *et al.*, A human-driven decline in global burned area. *Science* **356**, 1356–1362 (2017).
47. T. Xue *et al.*, Estimation of stillbirths attributable to ambient fine particles in 137 countries. *Nat. Commun.* **13**, 6950 (2022).
48. T. Xue *et al.*, Estimation of pregnancy losses attributable to exposure to ambient fine particles in south Asia: An epidemiological case-control study. *Lancet Planet. Health* **5**, e15–e24 (2021).
49. H. Zhang *et al.*, Ambient air pollution and stillbirth: An updated systematic review and meta-analysis of epidemiological studies. *Environ. Poll.* **278**, 116752 (2021).
50. T. Xue, T. Zhu, G. Geng, Q. Zhang, Association between pregnancy loss and ambient pm2.5 using survey data in Africa: A longitudinal case-control study, 1998–2016. *Lancet Planet. Health* **3**, e219–e225 (2019).
51. K. P. Vadrevu *et al.*, Trends in vegetation fires in south and southeast Asian countries. *Sci. Rep.* **9**, 1–13 (2019).
52. GB of Disease Collaborative Network, *Global Burden of Disease Study 2017 (GBD 2017) Results* (Institute for Health Metrics and Evaluation IHME, Seattle, WA, 2018).
53. O. Pechony, D. T. Shindell, Driving forces of global wildfires over the past millennium and the forthcoming century. *Proc. Natl. Acad. Sci. U.S.A.* **107**, 19167–19170 (2010).
54. C. Wu *et al.*, Historical and future global burned area with changing climate and human demography. *One Earth* **4**, 517–530 (2021).
55. ICF International, "Demographic and health survey sampling and household listing manual" (Technical Report, MEASURE DHS, Calverton, MD, 2012).
56. C. R. Burgert, J. Colston, T. Roy, B. Zachary, "Geographic displacement procedure and georeferenced data release policy for the Demographic and Health Surveys" (DHS Spatial Analysis Report No. 7, Technical Report, ICF International, Calverton, MD, 2013).
57. R. Burstein *et al.*, Mapping 123 million neonatal, infant and child deaths between 2000 and 2017. *Nature* **574**, 353–358 (2019).
58. Institute for Health Metrics and Evaluation, "Low- and middle-income country neonatal, infant, and under-5 mortality geospatial estimates 2000–2017" (GHDx, 2019).
59. National Institute of Statistics and Geography (INEGI), Registros Administrativos - Estadísticas (2020).
60. TSI Data Portal for Statistics, Infant mortality rate by province 2009–2019 (2019).
61. Y. Wang *et al.*, Under-5 mortality in 2851 Chinese counties, 1996–2012: A subnational assessment of achieving MDG 4 goals in China. *Lancet* **387**, 273–283 (2016).
62. Institute for Health Metrics and Evaluation (IHME), "Global burden of disease study 2017: All-cause mortality and life expectancy 1950–2017" (Technical Report, 2019).
63. WorldPop, Population counts (2016).
64. G. Otón, J. Lizundia-Loiola, M. L. Pettinari, E. Chuvieco, Development of a consistent global long-term burned area product (1982–2018) based on AVHRR-LTDR data. *Int. J. Appl. Earth Obs. Geoinf.* **103**, 102473 (2021).
65. G. Otón, "ESA Climate Change Initiative-Fire_cci D4. 2.2 Product User Guide-AVHRR-Long Term Data Record (PUG-LTDR)" (Technical Report, 2020).
66. G. Otón, R. Ramo, J. Lizundia-Loiola, E. Chuvieco, Global detection of long-term (1982–2017) burned area with AVHRR-LTDR data. *Remote Sens.* **11**, 2079 (2019).
67. G. Otón, M. Franquesa, J. Lizundia-Loiola, E. Chuvieco, "Validation of low spatial resolution and no-dichotomy global long-term burned area product by pareto boundary" in *Earth Resources and Environmental Remote Sensing/GIS Applications XII (SPIE, 2021)*, vol. 11863, pp. 293–299.
68. R. Ramo *et al.*, African burned area and fire carbon emissions are strongly impacted by small fires undetected by coarse resolution satellite data. *Proc. Natl. Acad. Sci. U.S.A.* **118**, e2011160118 (2021).
69. H. Hersbach *et al.*, The ERA5 global reanalysis. *Quart. J. R. Meteorol. Soc.* **146**, 1999–2049 (2020).
70. M. Burke, E. Gong, K. Jones, Income shocks and HIV in Africa. *Econ. J.* **125**, 1157–1189 (2015).
71. C. Perez-Heydrich, J. Warren, C. Burgert, M. Emch, "Guidelines on the use of DHS GPS data" (Spatial Analysis Reports No. 8, 2013).
72. H. K. Pullabhotla, M. Zahid, S. Heft-Neal, V. Rathi, M. Burke, Global biomass fires and infant mortality (Version v1) [Data set]. Zenodo. <https://doi.org/10.5281/zenodo.7854094>. Deposited 15 May 2023.